



UNIVERSITY OF LEEDS

This is a repository copy of *Impact of corrosion products on performance of imidazoline corrosion inhibitor on X65 carbon steel in CO<sub>2</sub> environments*.

White Rose Research Online URL for this paper:  
<https://eprints.whiterose.ac.uk/176177/>

Version: Accepted Version

---

**Article:**

Shamsa, A, Barker, R [orcid.org/0000-0002-5106-6929](https://orcid.org/0000-0002-5106-6929), Hua, Y [orcid.org/0000-0002-7457-1813](https://orcid.org/0000-0002-7457-1813) et al. (3 more authors) (2021) Impact of corrosion products on performance of imidazoline corrosion inhibitor on X65 carbon steel in CO<sub>2</sub> environments. *Corrosion Science*, 185. 109423. ISSN 0010-938X

<https://doi.org/10.1016/j.corsci.2021.109423>

---

© 2021, Elsevier. This manuscript version is made available under the CC-BY-NC-ND 4.0 license <http://creativecommons.org/licenses/by-nc-nd/4.0/>.

**Reuse**

This article is distributed under the terms of the Creative Commons Attribution-NonCommercial-NoDerivs (CC BY-NC-ND) licence. This licence only allows you to download this work and share it with others as long as you credit the authors, but you can't change the article in any way or use it commercially. More information and the full terms of the licence here: <https://creativecommons.org/licenses/>

**Takedown**

If you consider content in White Rose Research Online to be in breach of UK law, please notify us by emailing [eprints@whiterose.ac.uk](mailto:eprints@whiterose.ac.uk) including the URL of the record and the reason for the withdrawal request.



[eprints@whiterose.ac.uk](mailto:eprints@whiterose.ac.uk)  
<https://eprints.whiterose.ac.uk/>

# Impact of corrosion products on performance of imidazoline corrosion inhibitor on X65 carbon steel in CO<sub>2</sub> environments

Amir Shamsa<sup>a</sup>, Richard Barker<sup>a</sup>, Yong Hua<sup>a</sup>, Evgeny Barmatov<sup>b</sup>, Trevor L. Hughes<sup>b</sup>, Anne Neville<sup>a</sup>

<sup>a</sup>Institute of Functional Surfaces, School of Mechanical Engineering, University of Leeds, Leeds, LS2 9JT, UK

<sup>b</sup>Schlumberger Cambridge Research, Cambridge, CB3 0EL, UK

## Abstract

The impact of pre-corrosion on the performance of an imidazoline-based corrosion inhibitor was evaluated with respect to inhibition of uniform and localised corrosion in CO<sub>2</sub>-environments. Corrosion protection was found to be a function of two factors, inhibitor adsorption/film formation and presence of corrosion products. This effect was most significant in the presence of a continuous FeCO<sub>3</sub>-rich layer with high coverage of the steel surface, resulting in the inhibitor only providing ~25% of the overall protection afforded by the corrosion inhibitor and FeCO<sub>3</sub>. The presence of corrosion products had a significant influence on inhibitor adsorption and on corrosion pit depth.

**Key words:** CO<sub>2</sub> corrosion, imidazoline inhibitor, localised corrosion, iron carbonate

## 1.0 Introduction

In the oil and gas industry it has been estimated that 80% of failures during pipeline operations are corrosion-related, mainly due to the continued use of ferrous metallurgy which is not adequately protected [1]. It is extremely important to minimise any form of deterioration of equipment as this typically leads to shutdowns as a result of failures which impose unnecessary costs [1, 2]. The use of corrosion inhibitors has proven to be one of the most economically favourable methods to combat corrosion in the oil and gas industry [3, 4]. However, in addition to the cost of corrosion inhibitors, there are several other financial factors which are associated with the use of such chemicals. These include the capital cost of injection equipment as well as operational expenditure in relation to the maintenance and monitoring of residual inhibitor concentrations in active systems [1]. Corrosion mitigation using corrosion inhibitors might therefore only be deemed to be a cost-effective requirement several months or years after oil and gas production has commenced, either due to a natural increase in water cut within the produced

fluids or due to the use of water injection as a form of enhanced oil recovery, resulting in a greater production of corrosive reservoir waters [5].

In many cases, once the use of corrosion inhibitors has become a requirement, the pipeline has already corroded internally to a certain extent, and as a result, corrosion products have precipitated or accumulated onto the pipeline steel surfaces [6-8]. Conversely, the formation of corrosion products is also a possibility during periods of intermittent or insufficient inhibitor injection even when a corrosion inhibition strategy is employed on a facility. It is therefore of great importance to evaluate any possible antagonistic or synergistic effects associated with the use of corrosion inhibitors in the presence of such corrosion products within the expected environment in order to ensure that the corrosion threat is mitigated effectively, especially from the perspective of localised corrosion [1, 9]. It is important to be able to decouple the individual efficiencies of corrosion inhibitors and corrosion products in their ability to suppress the general and localised corrosion rates. This is challenging, but, extremely important in the context of determining the compatibility of corrosion inhibitors with such layers, as well as their ability to function in such environments and their mechanism(s) of inhibition [10, 11].

The effect of pre-corrosion on the performance of corrosion inhibitors was evaluated by Gulbrandsen *et al.* [12], who conducted a series of experiments on carbon steel in a CO<sub>2</sub>-saturated environment at 20-50°C. They concluded that the tested imidazoline-based corrosion inhibitor was incompatible with a cementite (Fe<sub>3</sub>C) layer which resulted in poor inhibition and localised attack in the form of pitting corrosion. Pre-corrosion periods of 10 and 14 days were found to lead to almost no inhibition efficiency as compared to 95% efficiency on wet-ground steel. Observations made by Paolinelli *et al.* [13] in a series of experiments conducted on carbon steel in a CO<sub>2</sub>-saturated environment at 40°C concluded that a protective inhibitor film was able to form in the presence of Fe<sub>3</sub>C and still greatly reduced the corrosion rate. Similarly, Zhang *et al.* [14] conducted a series of pre-corrosion experiments at 60°C with an extended study which was able to conclude that the formation of iron carbonate (FeCO<sub>3</sub>) had an obstructive influence on the performance of an imidazoline corrosion inhibitor. They found that 24 h pre-corrosion led to a 76% reduction in the inhibitor efficiency.

Existing literature has shown that the influence of pre-corrosion on inhibition has mainly been evaluated on non-protective crystalline corrosion products or in the presence of Fe<sub>3</sub>C with little attention on the performance of corrosion inhibitors with respect to the localised corrosion behaviour [15, 16]. The objectives of this work are to determine the ability of an imidazoline corrosion inhibitor to suppress the corrosion rate of three different types of pre-corroded carbon steel. These are characterised as; (i) Fe<sub>3</sub>C-rich layer, (ii) FeCO<sub>3</sub> layer with partial coverage of the

steel, and (iii)  $\text{FeCO}_3$  with full coverage of the steel. In addition, the study looks at the effect of the corrosion inhibitor on the morphology of the corrosion product layer, as well as the performance of the corrosion inhibitor in these environments with respect to both general and localised corrosion.

## 2.0 Experimental Procedure

### 2.1 Material preparation

Specimens were machined into 25 mm diameter, 6 mm thick coupons from a X65 carbon steel stock bar. A Kapton insulated wire was attached to each specimen using a two-component conductive glue to allow for electrochemical measurements during the experiments. The specimens were later embedded within a two-component epoxy resin resulting in a total exposed steel area of  $4.9 \text{ cm}^2$ . The specimen preparation process was conducted no more than 30 minutes prior to an experiment and consisted of successively wet-grinding each specimen with 120, 320 and finally with 600 silicon carbide (SiC) grit paper. This was then followed by rinsing the specimen with acetone and distilled water before gently drying using compressed air. The X65 carbon steel evaluated in this study possesses a ferritic-pearlitic microstructure (Figure 1) with the specified elemental composition provided in Table 1.

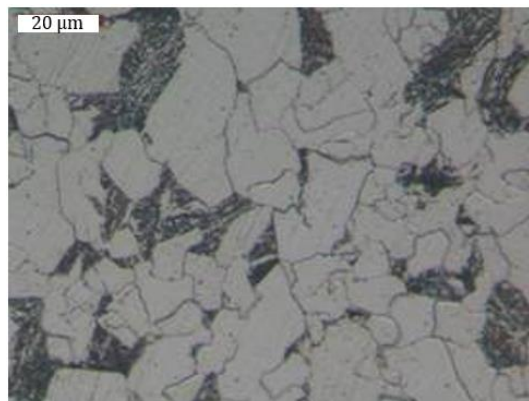


**Figure 1: X65 carbon steel microstructure**

**Table 1: Elemental composition of X65 steel (wt.%)**

<b>C</b>	<b>Si</b>	<b>Mn</b>	<b>P</b>	<b>S</b>	<b>Cr</b>	<b>Mo</b>	<b>Ni</b>
0.12	0.18	1.27	0.008	0.002	0.11	0.17	0.07
<b>Cu</b>	<b>Sn</b>	<b>Al</b>	<b>B</b>	<b>Nb</b>	<b>Ti</b>	<b>V</b>	<b>Fe</b>
0.12	0.008	0.022	0.0005	0.054	0.001	0.057	Balance

## 2.2 Brine preparation and chemical reagents

A 3 wt.% NaCl brine, prepared by dissolving analytical grade NaCl (Sigma-Aldrich) in distilled water was used. The brine solution was prepared at least 24 h in advance of each experiment. The brine was continuously bubbled with CO<sub>2</sub> overnight as well as during each experiment to ensure CO<sub>2</sub> saturation was achieved and maintained. For experiments where the corrosion inhibitor was used, the inhibitor was injected using a calibrated micro-pipette.

The composition of the imidazoline based corrosion inhibitor is shown in Figure 2. The inhibitor is manufactured in a two-stage process involving a double condensation reaction of diethylenetriamine (DETA) and tall oil fatty acid (TOFA). The inhibitor was supplied by M-I SWACO. <sup>1</sup>H and <sup>13</sup>C NMR spectroscopy (400 MHz, Bruker) was used to characterise the composition of the corrosion inhibitor mixture. The main components are the aminoethyl imidazoline (1) and its precursor, the amido-amine (2). The <sup>13</sup>C NMR spectrum (Figure 3) shows two strong signals associated with amide at 173.4 ppm and imidazoline signal at 168.0 ppm. Several sets of overlapped triplets are observed at 3.8-2.5 ppm associated with CH<sub>2</sub> protons belonging to imidazoline (1) and the amido-amine (2). Product (1) has the two CH<sub>2</sub> imidazoline protons at 3.68 ppm (t, J = 9.6 Hz) and at ~3.3 ppm and two CH<sub>2</sub> ethylamino protons at ~3.12 (t, J = 6.1 Hz) and ~2.8 ppm. Analysis of the ratio of protons (integrals) in the terminal methyl-CH<sub>3</sub> group to other characteristic protons of the inhibitor, e.g. δ=3.68 ppm for CH<sub>2</sub> in structure (1) suggest that the relative concentration of imidazoline (1) in the mixture is 55 %.

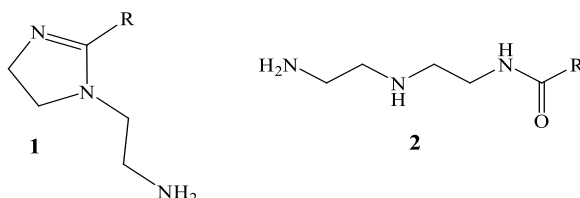
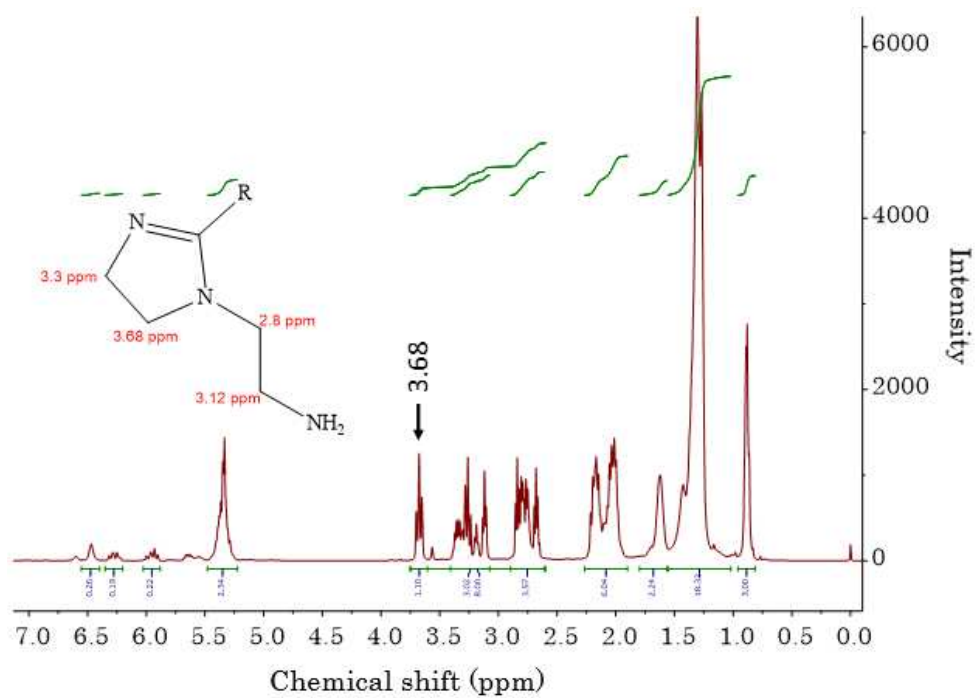
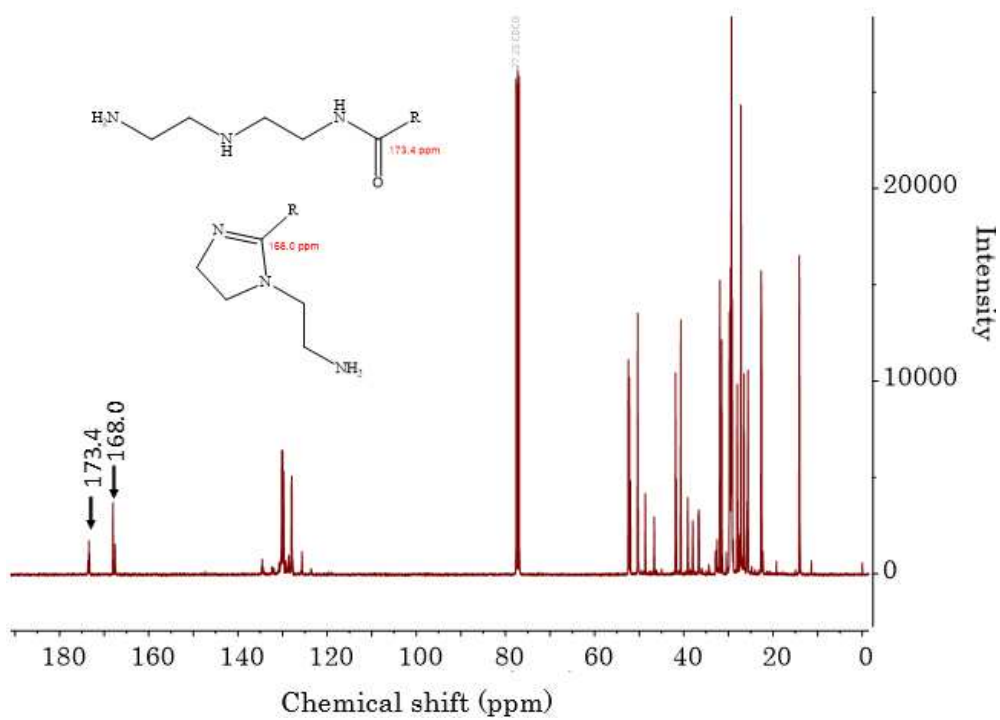


**Figure 2: Main components of a commercial imidazoline corrosion inhibitor based on the reaction of diethylene triamine (DETA) and tall oil fatty acid (TOFA): imidazoline (1) and amido-amine (2)**



(a)



(b)

Figure 3: <sup>1</sup>H (a) and <sup>13</sup>C (b) NMR spectra of the imidazoline-based corrosion inhibitor in CDCl<sub>3</sub>

### 2.3 Experimental method

The experimental procedure consisted of a two-stage process (Figure 4), where X65 carbon steel specimens were pre-corroded in autoclaves to generate three different surface conditions. The pre-corroded specimens were then characterised using X-ray diffraction (XRD), scanning electron microscopy (SEM), and surface profilometry in order to determine the corrosion products present, their morphology and the extent of localised corrosion on the surfaces, respectively. Remaining pre-corroded specimens which were not used for analysis were stored under vacuum before being transferred to glass cells and tested both in absence and presence of the imidazoline corrosion inhibitor, after which they were once again characterised using SEM, XRD and surface profilometry. This experimental procedure enabled the different corrosion product covered specimens to be tested with an inhibitor under identical initial brine chemistries, eliminating the effect of initial bulk pH observed during precipitation. This technique allowed for a more accurate performance evaluation and comparison between the different corrosion products.

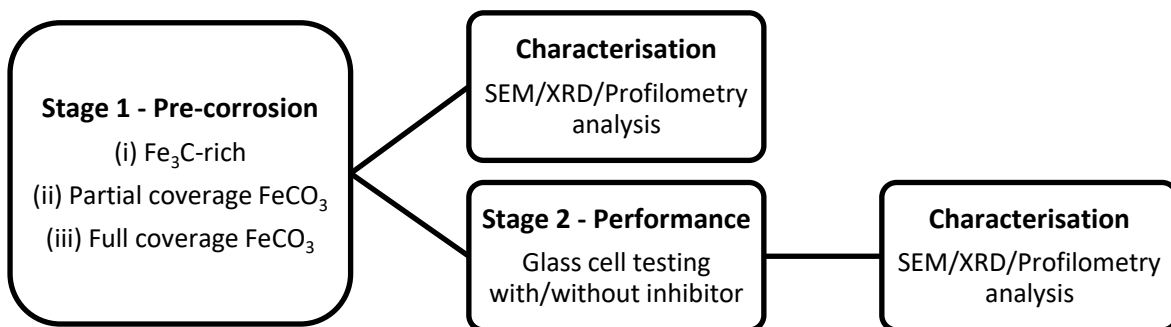


**Figure 4: Flow chart of experimental process**

#### 2.3.1 Autoclave pre-corrosion

Pre-corrosion of carbon steel specimens was done in an autoclave at 80°C for 6, 24 and 96 h in order to obtain carbon steel surfaces with an Fe<sub>3</sub>C rich layer, steel partially covered with FeCO<sub>3</sub> and steel fully covered with FeCO<sub>3</sub>, respectively. A full schematic representation of the autoclave setup is shown in Figure 5. Two X65 carbon steel specimens were attached to the autoclave specimen holders. The autoclave was equipped with a PTFE liner to prevent any galvanic effects through contact with the internal side walls of the autoclave during the pre-corrosion experiments. The pre-prepared, CO<sub>2</sub>-saturated brine solution was pumped into the autoclave at room temperature to achieve a surface area to volume ratio of 38.5 cm<sup>2</sup>/L. Autoclave inlet and outlet lines were then purged using CO<sub>2</sub> to remove any oxygen from the system. The autoclave was then heated to 80°C. When the entire experiment was completed, the autoclave was depressurised, and the specimens were removed. The specimens were then rinsed with distilled

water and dried using compressed air before being stored in a desiccator prior to transferring to a glass beaker set-up for further evaluation in both the absence and presence of the imidazoline corrosion inhibitor. The autoclave experimental parameters are provided in Table 2. It is important to highlight here that the experimental methodology was developed to focus on the corrosion product characteristics and their interaction with an imidazoline corrosion inhibitor. Hence, the purpose of the autoclave test methodology was to generate different pre-corroded specimens with different corrosion products or surface characteristics in a reasonable time frame.

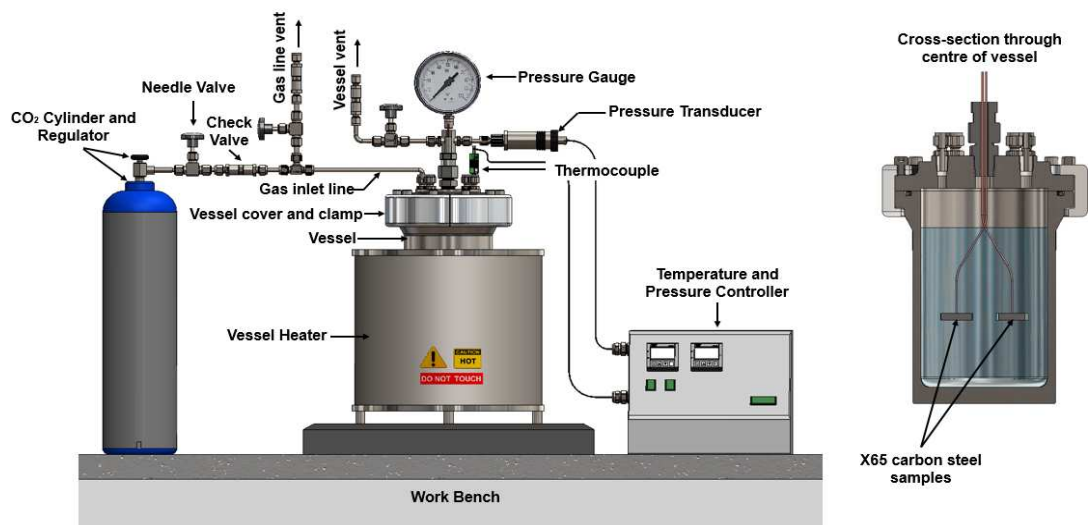


**Figure 5: Schematic of autoclave set-up for pre-corrosion of X65 carbon steel in CO<sub>2</sub>-environments at 80°C prior to transfer into glass cells for further study**

**Table 2: Autoclave pre-corrosion experimental parameters**

NaCl content (wt.%)	Temperature (°C)	Time (h)	$p_{\text{CO}_2}$ at 25°C (bar)	$p_{\text{CO}_2}$ at 80°C (bar)	$P_{\text{Total}}$ at 80°C (bar)	Initial brine pH
3	80	6, 24 and 96	0.98	1.4	1.9	4

### 2.3.2 Glass cell experiments

Pre-corroded X65 carbon steel specimens obtained from the autoclave experiments were immediately rinsed, dried, and stored in desiccators before being transferred and inserted into a glass cell (Figure 6) containing 1L of CO<sub>2</sub>-saturated 3 wt.% NaCl brine at 80°C. This was first performed in the absence of the corrosion inhibitor in order to establish a baseline of electrochemical and pH measurements for a total duration of 48 h, providing comparison for behaviour in the presence of the corrosion inhibitor. The exact same procedure was then repeated in the presence of the corrosion inhibitor, whereby the pre-corroded specimens were inserted into a CO<sub>2</sub>-saturated 3 wt.% NaCl brine already containing 30 ppm of the imidazoline

corrosion inhibitor. The total surface area to volume ratio was limited to 9.8 cm<sup>2</sup>/L in these experiments. Electrochemical and pH measurements were recorded throughout the glass cell experiments in order to monitor the specimen corrosion response and changes in bulk solution chemistry. Every experiment for each pre-corroded specimen was repeated at least twice to validate the results and to provide error bars for the electrochemical and pH measurements.

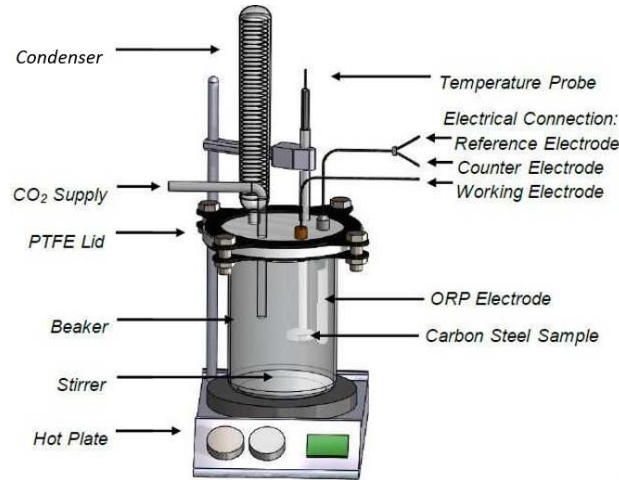


**Figure 6: Schematic of glass cell set-up for testing of pre-corroded X65 carbon steel in CO<sub>2</sub> environments at 80°C**

### 2.3.2.1 *In situ* electrochemical measurements

Electrochemical measurements were collected continuously in the glass cell experiments using the linear polarisation resistance (LPR) technique in order to evaluate the adsorption kinetics of the imidazoline corrosion inhibitor and are therefore presented as values of reciprocal of polarisation resistance. The corresponding corrosion rates were determined based on Stern-Geary coefficients of 25.5 and 14.4 mV obtained for uninhibited and inhibited (30 ppm) systems respectively at steady state (24 h) using wet-ground X65 steel. A three-electrode cell configuration was adopted which consisted of a working electrode and a combined redox electrode which comprised of a silver/silver chloride (Ag/AgCl) reference electrode (3M KCl) and a platinum auxiliary electrode. A carbon steel specimen was used as the working electrode which was polarised using an ACM Gill 8 potentiostat from -15 mV to +15 mV vs the open circuit potential (OCP). A scan rate of 0.25 mV/s was used with a 15 minute time interval between each LPR measurement. The end-point and integrated inhibitor efficiencies were determined using Eq. 1 and 2, respectively.

$$E_{Endpoint}(\%) = \left[ 1 - \left( \frac{R_{P,Uninhibited}}{R_{P,Inhibited}} \right) \right] \times 100 \quad Eq. 1$$

$$E_{Integrated}(\%) = \left[ 1 - \left( \frac{R_{P,Uninhibited}}{\int_0^{48} R_{P,Inhibited} dt} \right) \right] \times 100 \quad Eq. 2$$

where  $R_{P,Inhibited}$  is the inhibited polarisation resistance at the end of the test (ohm.cm<sup>2</sup>) and  $R_{P,Uninhibited}$  is the uninhibited polarisation resistance before inhibitor addition (ohm.cm<sup>2</sup>).

### 2.3.2.2 *In situ pH measurements*

The bulk solution pH was measured in the glass cell experiments using a Thermo Scientific Orion Star A211 benchtop meter with automatic temperature correction. The pH meter was calibrated before each measurement using pH 4, 7 and 10 buffer solutions. The pH probe was inserted into the experimental brine and left to reach a temperature of 80°C before a pH measurement was taken to reduce the experimental errors involved. The bulk solution pH was measured for repeat experiments from which an average was determined. Values of the maximum and minimum were represented by error bars.

## 2.4 Surface analysis methods

### 2.4.1 *Scanning electron microscopy (SEM)*

A Carl Zeiss EVO MA15 VP SEM instrument was used to provide secondary and backscattered top view imaging of the X65 carbon steel specimens. The specimens were carefully removed from the epoxy resins and were carbon coated along the height of their circumference to eliminate any surface charging effect before being inserted into the microscopy chamber. SEM analysis was used to visually characterise the corrosion products after removal from the autoclave and to assess the surface conditions after removal from the inhibited and uninhibited glass cells.

### 2.4.2 *X-ray diffraction (XRD)*

A Bruker D8 X-ray diffractometer was used for crystalline phase identification. The X65 carbon steel specimens were gently removed from their epoxy resins and inserted into a sample holder. A 10 x 10 mm surface coverage was achieved by the incident rays with scans ranging from a 2θ position of 20 to 70°. The total scan time was 50 minutes for each specimen. The XRD results were used to confirm the presence of crystalline corrosion products on carbon steel specimens after removal from the autoclave both before and after exposure to experimental brines (with and without inhibitor).

### 2.4.3 *NP<sub>FLEX</sub> 3D surface profilometry*

NP<sub>FLEX</sub> 3D surface profilometry was used to determine whether there was any form of localised corrosion attack on the carbon steel specimens after corrosion product precipitation in the autoclave experiments, as well as determining any increase or decrease in pit growth after

exposure to uninhibited and inhibited brines in the glass cell experiments. Carbon steel specimens were cleaned using Clarke's solution to remove any corrosion product on the steel surface or corrosion product within pits which may have accumulated during the corrosion experiments. The Clarke's solution was prepared (20 g antimony oxide + 50 g tin (II) chloride + 1000 ml hydrochloric acid) in accordance with ASTM Standard G1-03 [17]. Two 3 x 3 mm areas were scanned on two specimens for each experimental condition. A 2.5x objective was used with a working distance of approximately 3.5 mm. Vision 64 was then used to analyse the results where the average of the deepest 10 deepest pits across all regions was determined to represent the severity of the localised pitting attack. It should be noted that the error bars represent the range in the maximum pit depth across the scanned areas.

### 3.0 Results:

#### 3.1 Performance of imidazoline corrosion inhibitor on wet-ground X65 carbon steel

The performance of the imidazoline-based corrosion inhibitor was assessed on wet-ground X65 carbon steel in a previous study at 80°C [18]. The findings are summarised in Table 3. The reciprocal value of polarisation resistance ( $\frac{1}{R_p}$ ), corrosion rate and OCP as determined by electrochemistry for both inhibited and uninhibited wet-ground X65 at 80°C is provided in Table 3. Findings from the previous study indicated that  $\frac{1}{R_p}$  initially reduced in the presence of the corrosion inhibitor, from 13.29 to 6.94 milliohm<sup>-1</sup>cm<sup>-2</sup> (3.92 to 1.15 mm/year) in conjunction with an increase in the OCP of 23 mV (Table 3). The reciprocal of polarisation resistance continued to decrease with time and had stabilised at 0.96 milliohm<sup>-1</sup>cm<sup>-2</sup> (0.15 mm/year) after 48 h of exposure to the inhibited NaCl brine indicating adsorption onto the steel surface (Table 3), whereas in the absence of the corrosion inhibitor,  $\frac{1}{R_p}$  stabilised at 18.20 milliohm<sup>-1</sup>cm<sup>-2</sup> (5.37 mm/year). The reduction in  $\frac{1}{R_p}$  generated by the imidazoline corrosion inhibitor as a result of adsorption onto the steel surface resulted in an end-point efficiency of 92% with respect to uniform corrosion suppression. The bulk solution pH was measured *in situ* (Table 3) and indicated that the presence of the imidazoline corrosion inhibitor within the brine had resulted in a reduced rate of increase in the bulk pH, which then remained lower for the duration of the experiment, reaching 4.3 as compared to 5.5 at the end of the uninhibited experiment (Table 3). The localised corrosion behaviour was analysed using non-contact surface profilometry. The data provided (Table 3) is based on the deepest 10 pits averaged across two 3 × 3 mm areas on two specimens. The results indicated that the pit depth had dramatically reduced from 26.1<sup>+5.0</sup><sub>-2.3</sub> μm

(4.76 mm/year) to  $1.2_{-0.1}^{+0.1}$   $\mu\text{m}$  (0.22 mm/year) in the presence of the imidazoline corrosion inhibitor. The localised corrosion inhibitor efficiency was calculated using Eq. 3:

$$E_{pit}(\%) = \left(1 - \frac{P_{Inhibited}}{P_{Uninhibited}}\right) \times 100 \quad Eq. 3$$

where  $P_{Inhibited}$  is the pit depth after exposure to the inhibited brine ( $\mu\text{m}$ ) and  $P_{Uninhibited}$  is the pit depth after exposure to the uninhibited brine ( $\mu\text{m}$ ). This resulted in a localised corrosion inhibitor efficiency of 95.4%, which was greater than the uniform inhibitor efficiency of 92%.

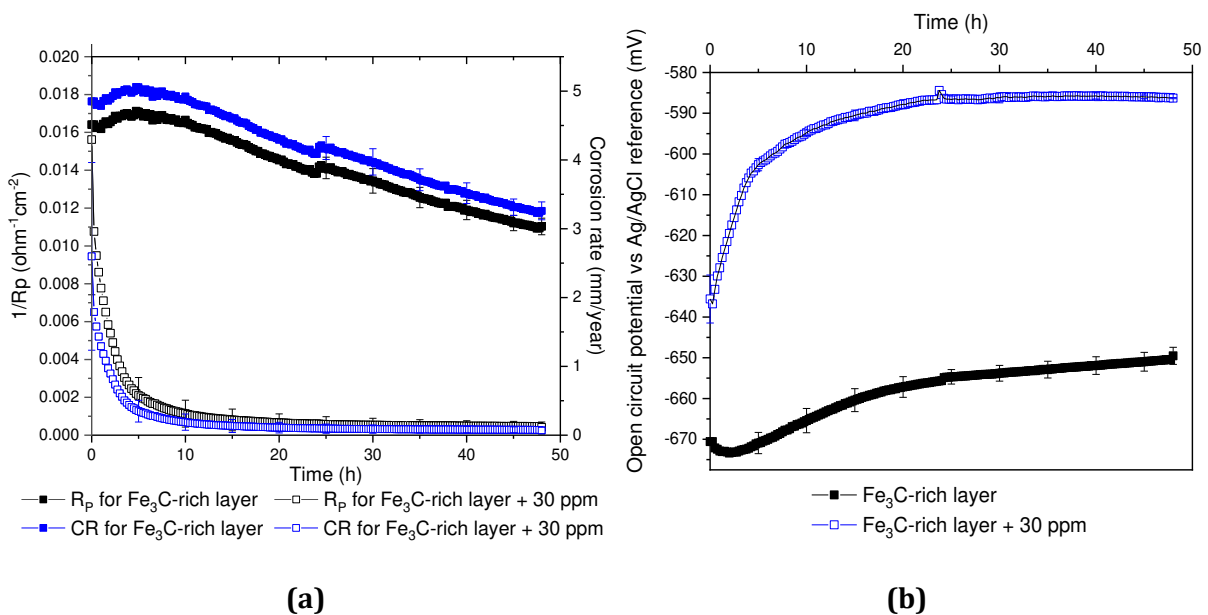
**Table 3: Corrosion response of imidazoline corrosion inhibitor on wet-ground X65 steel [18]**

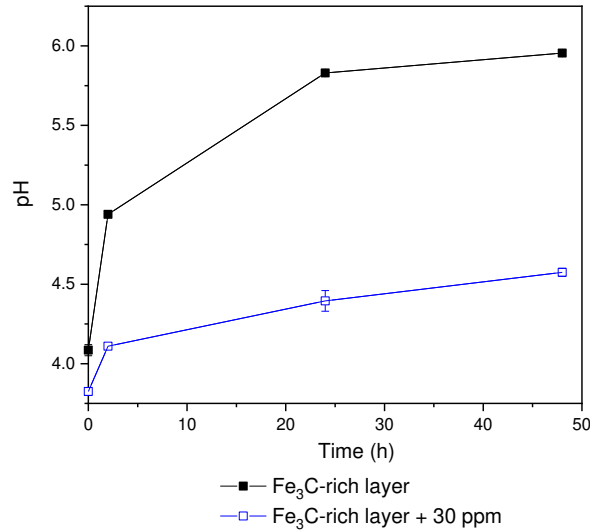
	Time (h)	1/R <sub>p</sub> (milliohm <sup>-1</sup> cm <sup>-2</sup> )	OCP (mV)	pH	Pit depth ( $\mu\text{m}$ )	E <sub>Uniform</sub> (%)	E <sub>Localised</sub> (%)
<b>Uninhibited wet-ground X65</b>	0	13.29	-687.15	4.1			
	1	14.98	-682.51	-			
	2	16.47	-680.85	4.5			
	5	17.85	-676.78	-			
	10	19.03	-669.04	-			
	24	18.85	-653.19	5.3			
	48	18.20	-648.58	5.5	26.1		
	<b>Inhibited (30 ppm) from 0 h</b>	0	6.94	-663.82	4.0		
1		4.82	-638.72	-			
2		3.04	-636.28	4.1			
5		1.57	-641.89	-			
10		1.29	-643.12	-			
24		1.19	-640.90	4.3			
48		0.96	-642.14	4.3	1.2	92.0	95.4

### 3.2 Performance of imidazoline corrosion inhibitor on an iron carbide (Fe<sub>3</sub>C) rich layer

A Fe<sub>3</sub>C-rich layer was allowed to reveal itself on X65 carbon steel by pre-corrosion in the autoclave at 80°C for 6 h, as described in section 2.3. The influence of the Fe<sub>3</sub>C-rich layer on the steel dissolution characteristics was evaluated using electrochemical measurements in the absence and presence of 30 ppm of the imidazoline corrosion inhibitor. The reciprocal values of polarisation resistance, corrosion rate and OCP, as determined by the LPR technique are provided in Figure 7. The reciprocal values of resistance for the uninhibited test specimen with the Fe<sub>3</sub>C-rich layer decreased from 16 to 12 milliohm<sup>-1</sup>cm<sup>-2</sup> (4.84 to 3.25 mm/year), (Figure 7(a)), most likely attributed to a significant increase in the bulk pH with time which increased from 4.1 to 6 after 48 h of exposure (Figure 7(c)) as compared to a bulk pH of 5.5 for the tests with initially wet-ground X65 specimens (Table 3). The greater increase in pH observed in the uninhibited Fe<sub>3</sub>C test is due to the greater rate of corrosion of the X65 carbon steel substrate, and hence greater

Fe<sup>2+</sup> release over the duration of the experiment. The reciprocal values of polarisation resistance (Figure 7(a)) showed that there was an immediate reduction in X65 corrosion rate in the presence of the inhibitor, which reduced with time from 16 milliohm<sup>-1</sup>cm<sup>-2</sup> (2.59 mm/year) at 0 h to 0.4 milliohm<sup>-1</sup>cm<sup>-2</sup> (0.07 mm/year) at 48 h as compared to 12 milliohm<sup>-1</sup>cm<sup>-2</sup> (3.25 mm/year) in the absence of corrosion inhibitor after 48 h of exposure. The presence of the imidazoline corrosion inhibitor resulted in a positive shift in the OCP of 35 mV in the beginning of the test which continued to increase throughout the duration of the experiment, reaching a stable potential of -585 mV as compared to -650 mV in the absence of the imidazoline corrosion inhibitor (Figure 7(b)). The inhibited test produced a lower pH at the end of the experiment (pH 4.5) compared with the uninhibited system (pH 6), (Figure 7(c)) both of which were comparable with the wet-ground X65 steel response in the presence and absence of the inhibitor (Table 3). The rate of reduction in the reciprocal value of polarisation resistance for the inhibited Fe<sub>3</sub>C-rich layer was lower in comparison to inhibited wet-ground X65 which indicated a slower rate of adsorption due to the presence of Fe<sub>3</sub>C. The imidazoline corrosion inhibitor was found to provide slightly greater protection in the presence of the Fe<sub>3</sub>C film (95% uniform end-point efficiency) as compared to 92% on wet-ground X65 steel, however, this could be partly attributed to the greater increase of bulk pH in the 48 h test period (Table 3 and Figure 7(c)), reducing the corrosivity of the test fluid.

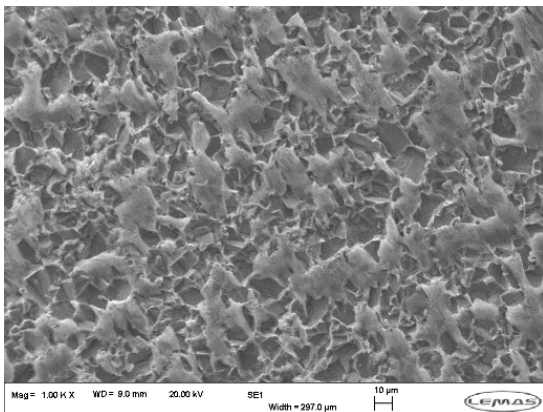




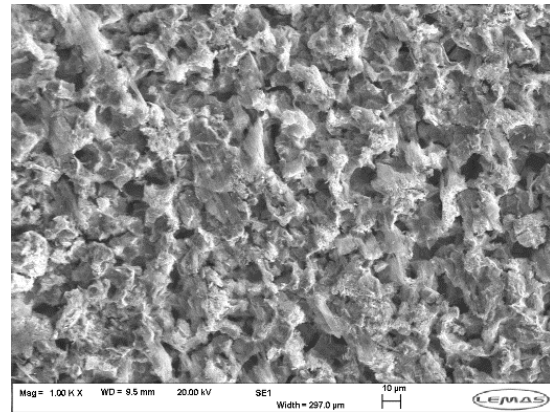
(c)

**Figure 7: (a) Reciprocal values of polarisation resistance, (b) OCP vs Ag/AgCl reference and (c) bulk pH as a function of time for X65 carbon steel (with a pre-formed Fe<sub>3</sub>C-rich layer) exposed to inhibited (30 ppm) and uninhibited CO<sub>2</sub>-saturated 3 wt.% NaCl solution at 80°C for 48 h. Note that inhibitor addition was performed prior to immersion of the specimen in the electrolyte.**

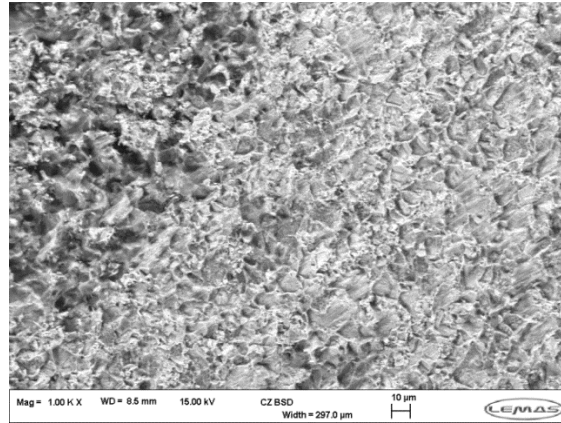
Top-view SEM images of the Fe<sub>3</sub>C layer before and after exposure to the uninhibited and inhibited NaCl based brines at 80°C (Figure 8) confirmed that the steel substrate had continued to corrode significantly in the uninhibited glass cell tests (Figure 8(b)), and also that less corrosion had occurred in the presence of the inhibitor (Figure 8(c)). However there were strong indications of non-uniform coverage of the inhibitor as variability in the extent of corrosion on the steel surface could be observed (Figure 8(c)).



(a)



(b)



(c)

**Figure 8: SEM top-view images for (a) Fe<sub>3</sub>C-rich layer on X65 carbon steel formed from 6 h pre-corrosion in autoclave at 80°C, (b) Fe<sub>3</sub>C-rich layer on X65 carbon steel after exposure to uninhibited CO<sub>2</sub>-saturated 3 wt.% NaCl brine at 80°C for 48 h and (c) Fe<sub>3</sub>C-rich layer on X65 carbon steel after exposure to inhibited (30 ppm) CO<sub>2</sub>-saturated 3 wt.% NaCl brine at 80°C for 48 h**

X-ray diffraction confirmed that no crystalline corrosion products were present after revealing the Fe<sub>3</sub>C layer in the autoclave (Figure 9(a)) or after exposure to either uninhibited or inhibited brines in the glass cell tests (Figure 9(b)-(c)).

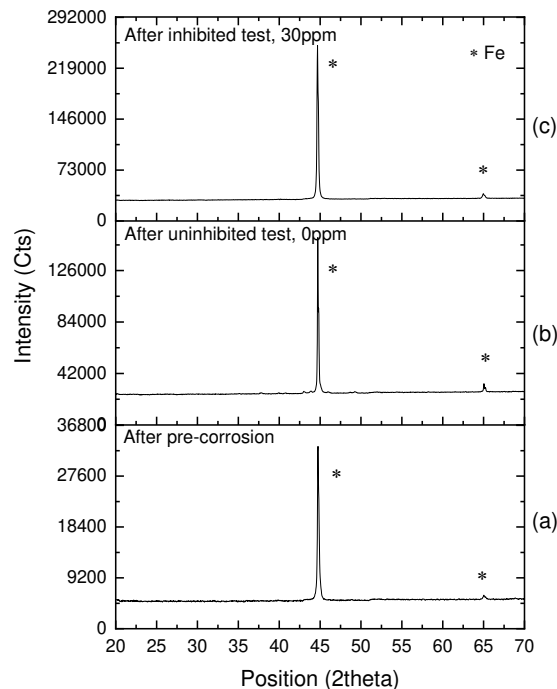


**Figure 9: XRD pattern for (a) Fe<sub>3</sub>C-rich layer on X65 carbon steel after 6 h pre-corrosion in autoclave at 80°C, (b) Fe<sub>3</sub>C-rich layer on X65 carbon steel after exposure to uninhibited**

**CO<sub>2</sub>-saturated 3 wt.% NaCl brine at 80°C for 48 h and (c) Fe<sub>3</sub>C-rich layer on X65 carbon steel after exposure to inhibited (30 ppm) CO<sub>2</sub>-saturated 3 wt.% NaCl brine at 80°C for 48 h**

The extent of localised corrosion was quantified using non-contact profilometry (Figure 10). The pit depth was evaluated and compared for the steel with the Fe<sub>3</sub>C-rich layer after pre-corrosion in the autoclave and after 48 h exposure to uninhibited and inhibited glass cell tests. The results indicate that the pit depth was  $9.0^{+1.4}_{-0.5}$   $\mu\text{m}$  (13.14 mm/year) after removal from the autoclave and increased to  $28.0^{+3.8}_{-1.9}$   $\mu\text{m}$  (3.46 mm/year) in the uninhibited glass cell tests (Figure 10). There was a smaller pit depth for the inhibited glass cell tests, where the pit depth had increased only to a value of  $11.0^{+2.4}_{-1.7}$   $\mu\text{m}$  (0.36 mm/year). The efficiency of the imidazoline corrosion inhibitor in providing protection to the Fe<sub>3</sub>C-rich steel substrate was determined using Equation 3.

The inhibitor efficiency in terms of localised corrosion was found to be 60.7% as compared to a uniform efficiency of 95% on the pre-corroded Fe<sub>3</sub>C-rich layer. This indicates that pre-corrosion of the Fe<sub>3</sub>C-rich layer can lead to similar inhibitor efficiency in terms of uniform corrosion (92 to 95), however a significant reduction of inhibitor efficiency in terms of localised corrosion (95.4 to 60.7%) compared to wet-ground X65 carbon steel. This is believed to be predominantly due to the slower adsorption in the presence of Fe<sub>3</sub>C as indicated by Figure 7.

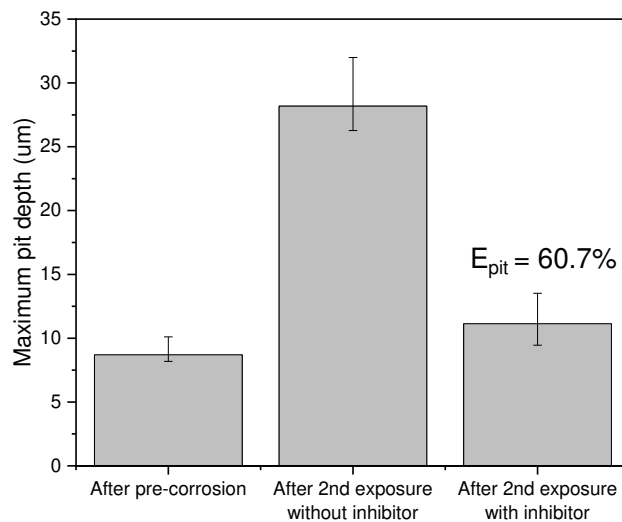


**Figure 10: Pit depth for Fe<sub>3</sub>C-rich layer on X65 carbon steel formed from 6 h pre-corrosion in autoclave at 80°C, Fe<sub>3</sub>C-rich layer on X65 carbon steel after exposure to uninhibited CO<sub>2</sub>-saturated 3 wt.% NaCl brine at 80°C for 48 h and Fe<sub>3</sub>C-rich layer on X65 steel after exposure to inhibited (30 ppm) CO<sub>2</sub>-saturated 3 wt.% NaCl brine at 80°C for 48 h**

### 3.3 Performance of imidazoline corrosion inhibitor on steel with partial iron carbonate ( $\text{FeCO}_3$ ) coverage

Pre-corrosion of X65 steel for 24 h at 80°C in an autoclave led to the precipitation of a  $\text{FeCO}_3$  layer which partially covered the steel surface and offered poor general corrosion protection to the substrate. The corrosion behaviour of the partially covered steel was evaluated using glass cells containing a  $\text{CO}_2$ -saturated 3 wt.% NaCl solution with and without 30 ppm of the imidazoline corrosion inhibitor to determine the efficiency compared to a wet-ground X65 steel surface, and a 6 h pre-corroded specimen with an  $\text{Fe}_3\text{C}$ -rich layer. The reciprocal values of polarisation resistance in the uninhibited system (Figure 11(a)) showed a decrease as a function of time which is believed to be predominantly as a result of the increase in the bulk solution pH due to an increase in  $\text{Fe}^{2+}$  ions in the bulk solution with time (Figure 11(c)). The reciprocal values of polarisation resistance in the inhibited test showed a relatively slow reduction during the 48 h test, where it decreased from 16 to 0.48 milliohm $^{-1}\text{cm}^{-2}$  (1.83 to 0.08 mm/year) after 48 h of exposure (Figure 11(a)) which occurred in conjunction with a positive shift in the OCP from -640 to -600 mV. The rate of decrease in  $\frac{1}{R_p}$  with time for the inhibited test was slower than that of wet-ground X65 steel and the pre-corroded  $\text{Fe}_3\text{C}$ -rich layer previously discussed.

These findings indicate that the presence of a crystalline corrosion product further hinders the adsorption kinetics and formation of the inhibitor film at the steel substrate. The bulk solution pH remained lower for the inhibited experiment throughout the duration of the tests (Figure 11(c)) due to a reduction in the number of  $\text{Fe}^{2+}$  ions released into the bulk solution as a result of the suppression of the corrosion rate. The end-point efficiency in terms of uniform corrosion was 96% which is comparable to the 92 and 95% end-point efficiencies obtained for wet-ground X65 and X65 with a  $\text{Fe}_3\text{C}$ -rich layer respectively, once the greater evolution of the bulk solution pH is taken into consideration. This indicated that although the adsorption of the corrosion inhibitor was hindered by the crystalline  $\text{FeCO}_3$  layer, the efficiency in terms of overall suppression of uniform corrosion was comparable after 48 h of exposure. The integrated efficiency of the uniform corrosion behaviour will be discussed in section 3.5.

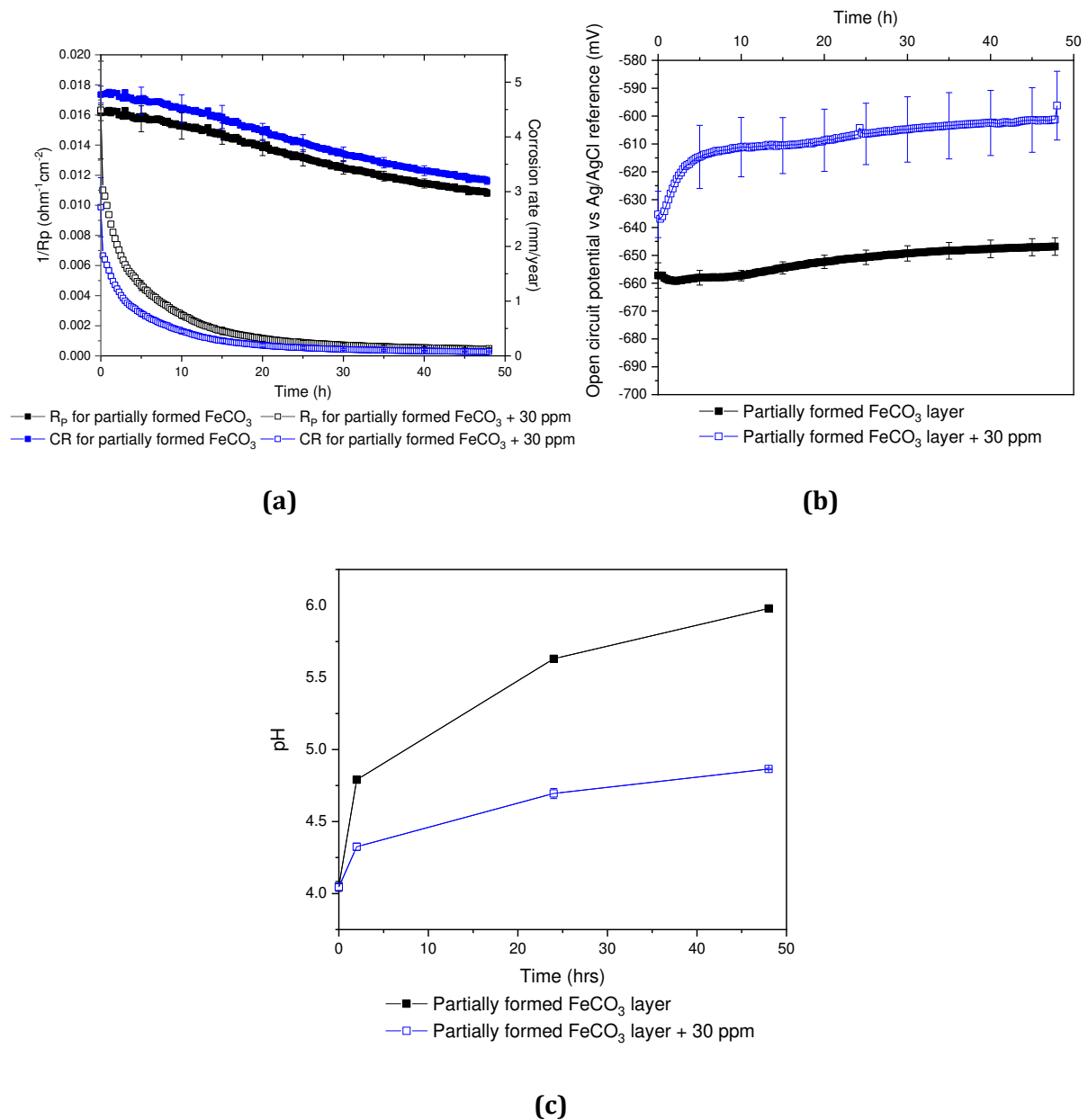
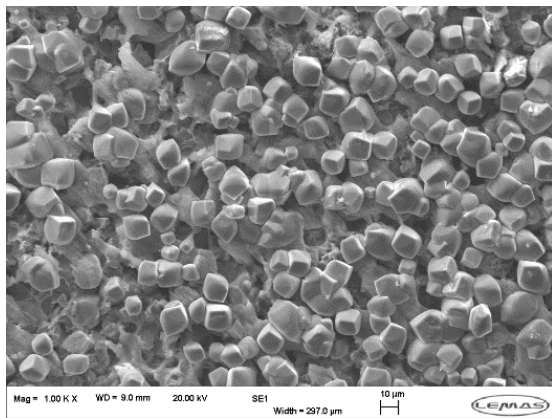


**Figure 11: (a) Reciprocal values of polarisation resistance, (b) OCP vs Ag/AgCl reference and (c) bulk pH as a function of time for X65 carbon steel (with a pre-formed partial coverage  $\text{FeCO}_3$  layer) exposed to inhibited (30ppm) and uninhibited  $\text{CO}_2$ -saturated 3 wt.% NaCl brines at  $80^\circ\text{C}$  for 48 h. Note that inhibitor addition was performed prior to immersion of the specimen in the electrolyte.**

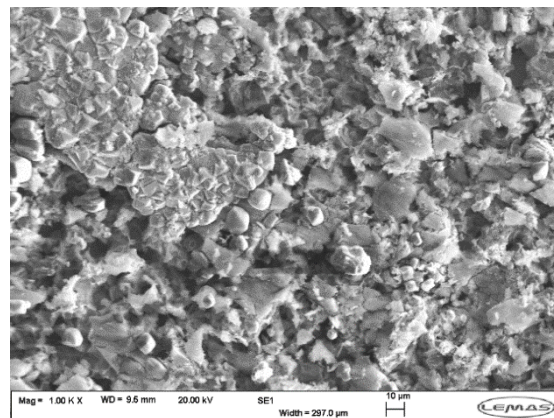
Examination of the X65 carbon steel surfaces post precipitation in the autoclave (Figure 12(a)) and after the glass cell tests with and without the imidazoline corrosion inhibitor (Figure 12(b-c)) showed that most of the  $\text{FeCO}_3$  had dissolved by the end of the 48 h uninhibited glass cell tests (Figure 12(b)), however there remained some areas with individual  $\text{FeCO}_3$  crystals and minor areas where the  $\text{FeCO}_3$  crystals had aggregated to form a conglomerate of crystals. In glass cell

tests with 30 ppm of the imidazoline corrosion inhibitor, it was confirmed that there had been further dissolution of the  $\text{FeCO}_3$  corrosion product where neither single crystals nor conglomerates of  $\text{FeCO}_3$  crystals could be visually identified (Figure 12(c)).

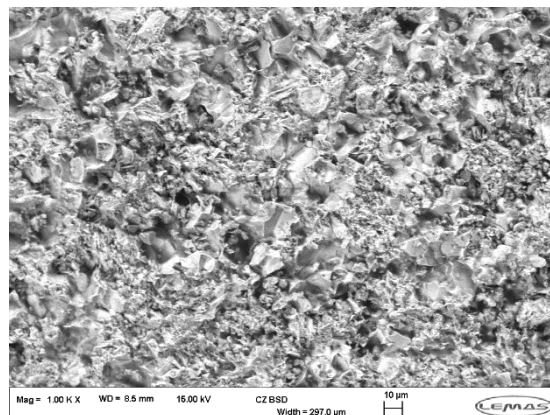
X-ray diffraction of the partially  $\text{FeCO}_3$  covered steel before and after exposure to uninhibited and inhibited brines (Figure 13) confirmed that  $\text{FeCO}_3$  was present after precipitation in the autoclaves (Figure 13(a)). However, after exposure to the uninhibited brine, only a small [104]  $\text{FeCO}_3$  peak was present which confirmed that most of the  $\text{FeCO}_3$  had dissolved in the absence of the corrosion inhibitor (Figure 13(b)). In the presence of the corrosion inhibitor there was no longer a  $\text{FeCO}_3$  peak present which confirmed that there had been further dissolution as suggested by the SEM images (Figure 12). However as a result of the gradual dissolution of  $\text{FeCO}_3$  during the 48 h test in the presence of the corrosion inhibitor, it was possible for the corrosion inhibitor to adsorb onto the steel surface which had been previously occupied by  $\text{FeCO}_3$  crystals as indicated by the gradual reduction in reciprocal values of polarisation resistance in Figure 11.



(a)



(b)



(c)

**Figure 12: SEM top-view images for (a) X65 carbon steel after 24 h pre-corrosion in autoclave at 80°C, (b) 24 h pre-corroded steel specimen after exposure to uninhibited**

**CO<sub>2</sub>-saturated 3 wt.% NaCl brine at 80°C for 48 h and (c) 24 h pre-corroded steel specimen after exposure to inhibited (30 ppm) CO<sub>2</sub>-saturated 3 wt.% NaCl brine at 80°C for 48 h**

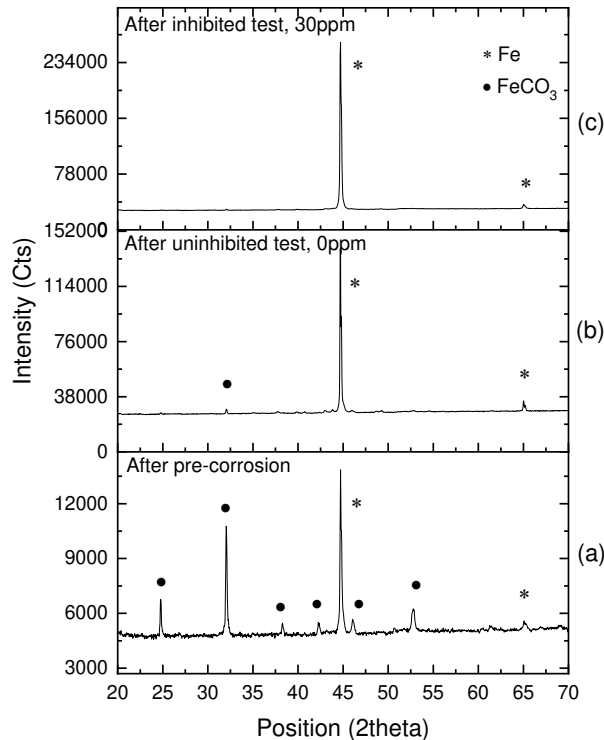


**Figure 13: XRD pattern for (a) X65 carbon steel after 24 h pre-corrosion in autoclave at 80°C, (b) 24 h pre-corroded steel specimen after exposure to uninhibited CO<sub>2</sub>-saturated 3 wt.% NaCl brine at 80°C for 48 h and (c) 24 h pre-corroded steel specimen after exposure to inhibited (30 ppm) CO<sub>2</sub>-saturated 3 wt.% NaCl brine at 80°C for 48 h**

The extent of localised corrosion on the pre-corroded specimens with the partial coverage of FeCO<sub>3</sub> were evaluated using non-contact profilometry before and after exposure to uninhibited and inhibited glass cell experiments (Figure 14). The pit depth was  $26.0^{+4.2}_{-1.9}$  μm (9.49 mm/year) for the pre-corroded layer prior to glass cell testing and was found to have remained fairly stable at a pit depth of  $25.5^{+2.9}_{-1.7}$  μm after exposure to the uninhibited glass cell test which was within the experimental error. However after glass cell testing with the corrosion inhibitor, the pit depth had increased to  $34.0^{+20}_{-10}$  μm (1.46 mm/year), resulting in a localised inhibitor efficiency of -33.3% as compared to a uniform end-point efficiency of 96.0% which provides further indication that pre-corrosion can lead to improved uniform corrosion efficiency however at the cost of a dramatic reduction in the inhibitors localised corrosion efficiency, indicating an antagonistic interaction between the corrosion inhibitor and the FeCO<sub>3</sub> corrosion product. It should be noted once again that the provided pit depths are representative of an average taken of the 10 deepest

pits taken across two different scanned 3×3 mm areas across two different specimens and as a result the error bars represent the range in the maximum pit depth across the scanned areas.

The negative average efficiency of the corrosion inhibitor indicates that the corrosion inhibitor is unable to inhibit localised corrosion when used on X65 surfaces with partial coverage of FeCO<sub>3</sub>. As previously discussed, most of the FeCO<sub>3</sub> had completely dissolved by the end of the 48 h inhibited tests (Figure 12-13) however it is unclear exactly how long it had taken to dissolve and whether or not there was any FeCO<sub>3</sub> present within the pits. It is therefore possible that FeCO<sub>3</sub> present within the pits could have hindered local adsorption of the corrosion inhibitor which resulted in further pit growth and/or the FeCO<sub>3</sub> on the surface hindered local adsorption of the corrosion inhibitor before it completely dissolved, resulting in pit initiation and/or continued growth of existing pits.

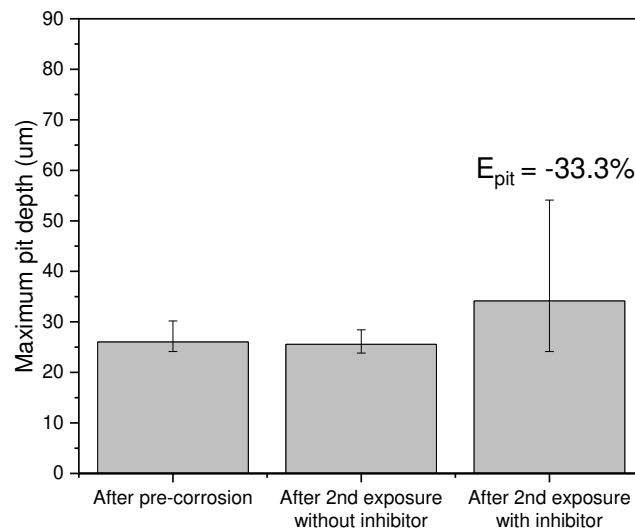
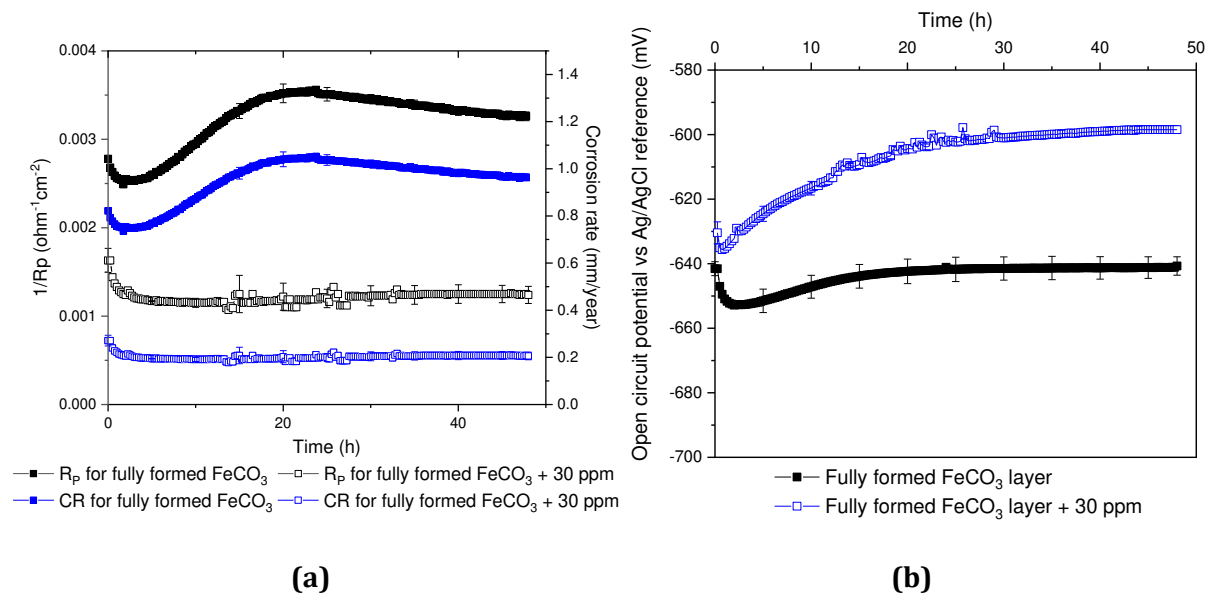


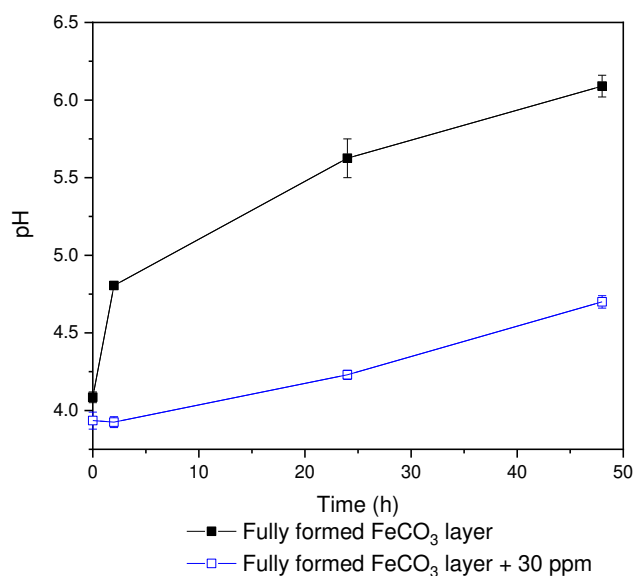
**Figure 14: Pit depth for partial coverage FeCO<sub>3</sub> layer after 24 h pre-corrosion in autoclave at 80°C, partial coverage FeCO<sub>3</sub> layer after uninhibited exposure to 3 wt.% NaCl brine at 80°C for 48 h and partial coverage FeCO<sub>3</sub> layer after exposure to 30 ppm inhibited 3 wt.% NaCl brine at 80°C for 48 h**

### 3.4 Performance of imidazoline corrosion inhibitor on X65 steel with full iron carbonate (FeCO<sub>3</sub>) coverage

A FeCO<sub>3</sub> corrosion product providing significant coverage and protection to the X65 steel specimen was generated in autoclaves after 96 h pre-corrosion. Again, these specimens were transferred to glass cell experiments in uninhibited and inhibited CO<sub>2</sub>-saturated 3 wt.% NaCl brines and their corrosion response was assessed using the linear polarisation resistance technique (Figure 15). The uninhibited glass cell experiments on the FeCO<sub>3</sub> covered steel surfaces indicated that the reciprocal value of polarisation resistance initially started to increase before

stabilising and slowly decreasing after 20 h of exposure to the uninhibited brine (Figure 15(a)). The increase in the reciprocal value of polarisation resistance was a possible indication of dissolution of the  $\text{FeCO}_3$  corrosion product layer which had a subsequent effect of increasing the bulk solution pH (Figure 15(c)), which was 5.6 after 24 h of exposure. The progressive increase in pH then led to a relatively slow decline in the corrosion rate (Figure 15(a)). The reciprocal values of polarisation resistance for the fully  $\text{FeCO}_3$  covered steel surface exposed to the inhibited brine solution were lower than that of the uninhibited glass cell experiment (both at the start and end of the experiment), stabilising faster (within 3 h) at a value of  $1.25 \text{ milliohm}^{-1}\text{cm}^{-2}$  ( $0.2 \text{ mm/year}$ ) as compared to a maximum value of  $3.5 \text{ milliohm}^{-1}\text{cm}^{-2}$  ( $1 \text{ mm/year}$ ) for the uninhibited glass cell test (Figure 15(a)). The OCP shifted positively by 40 mV after 48 h of exposure to the inhibited brine (Figure 15(b)). The end-point uniform corrosion efficiency was 83% which was significantly lower than the previously discussed uniform corrosion efficiencies observed for wet-ground X65 steel, 6 h pre-corroded X65 and 24 h pre-corroded X65 (92, 95 and 96% respectively). This is attributed to the presence of a fully developed  $\text{FeCO}_3$  layer which limits transport and adsorption of an inhibitor film onto the steel substrate.

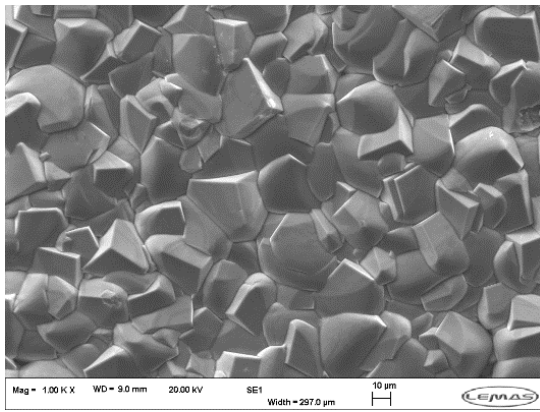




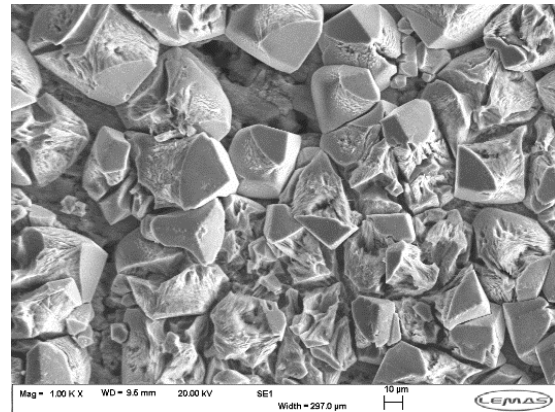
(c)

**Figure 15: (a) Reciprocal values of polarisation resistance, (b) OCP vs Ag/AgCl reference and (c) bulk pH as a function of time for X65 carbon steel (with a pre-formed full coverage FeCO<sub>3</sub> layer) exposed to inhibited and uninhibited CO<sub>2</sub>-saturated 3 wt.% NaCl brines at 80°C for 48 h. Note that inhibitor addition was performed prior to immersion of the specimen in the electrolyte.**

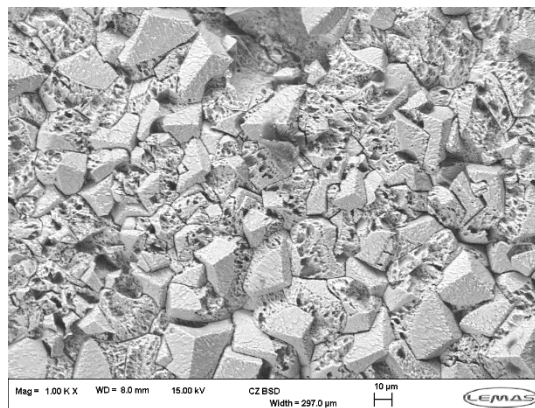
Top-view images from the SEM for the FeCO<sub>3</sub> covered specimens before and after exposure to the uninhibited and inhibited glass cell tests (Figure 16) confirmed that the corrosion product layer had been slowly dissolving in both uninhibited and inhibited glass cell tests (Figure 16(b-c)). The dissolution led to an increase in both primary and secondary porosity (intergranular porosity and single crystal porosity, respectively) which led to a reduction in corrosion protection offered by the corrosion product layer. The increase in porosity both within and around the FeCO<sub>3</sub> crystals may also have been a significant factor influencing the localised corrosion behaviour which will be further discussed later.



(a)



(b)



(c)

**Figure 16: SEM top-view images for (a) X65 carbon steel after 96 h pre-corrosion in autoclave at 80°C, (b) 96 h pre-corroded steel specimen after exposure to uninhibited CO<sub>2</sub>-saturated 3 wt.% NaCl brine at 80°C for 48 h and (c) 96 h pre-corroded steel specimen after exposure to inhibited (30 ppm) CO<sub>2</sub>-saturated 3 wt.% NaCl brine at 80°C for 48 h**

XRD patterns corresponding to the FeCO<sub>3</sub> covered steel specimens before and after exposure to the uninhibited and inhibited glass cell environments (Figure 17) confirmed that crystalline FeCO<sub>3</sub> was still present on the X65 carbon steel surfaces after exposure to both the uninhibited and inhibited glass cell tests. The pit depth was evaluated and compared for the FeCO<sub>3</sub> covered X65 specimens before and after exposure to the uninhibited and inhibited glass cell tests (Figure 18) using non-contact surface profilometry. The data shows that the pit depth after precipitation of the corrosion product layer in the autoclave was  $46.0 \pm_{-4}^{8.6} \mu\text{m}$  (4.19 mm/year) which then increased to  $51.0 \pm_{-10}^{11.9} \mu\text{m}$  (0.91 mm/year) and  $54.0 \pm_{-7.4}^{28} \mu\text{m}$  (1.46 mm/year) after exposure to the uninhibited and inhibited glass cell tests, respectively (Figure 18). The pit depth was greater after glass cell testing in the inhibited brine as compared to after testing in the uninhibited brine which

suggests that the inhibitor did not inhibit localised corrosion attack. The efficiency of the corrosion inhibitor with respect to the localised corrosion behaviour calculated using Equation 3 was -5.9% (Figure 18) which confirmed that the inhibitor did not provide any significant additional protection against localised corrosion. This is believed to be due to the presence of a crystalline corrosion product layer ( $\text{FeCO}_3$ ) which fully covered the steel surface. As previously discussed, it is important to note that the error bars in Figure 18 represent the range in the maximum pit depth which significantly increased after exposure to the inhibited brine indicating that the actual measured maximum pit depth had also significantly increased. The reduced ability of the corrosion inhibitor in providing protection against localised corrosion can in this case be partly attributed to the porous nature of the  $\text{FeCO}_3$  layer by the end of the 48 h inhibited test (Figure 16), where the inhibitor appears to be unable to function in local environments under  $\text{FeCO}_3$  crystals. It can also be attributed to the possibility of  $\text{FeCO}_3$  being present within existing pits after the autoclave pre-corrosion period which limits the accessibility of the corrosion inhibitor to these local sites on the steel surface.

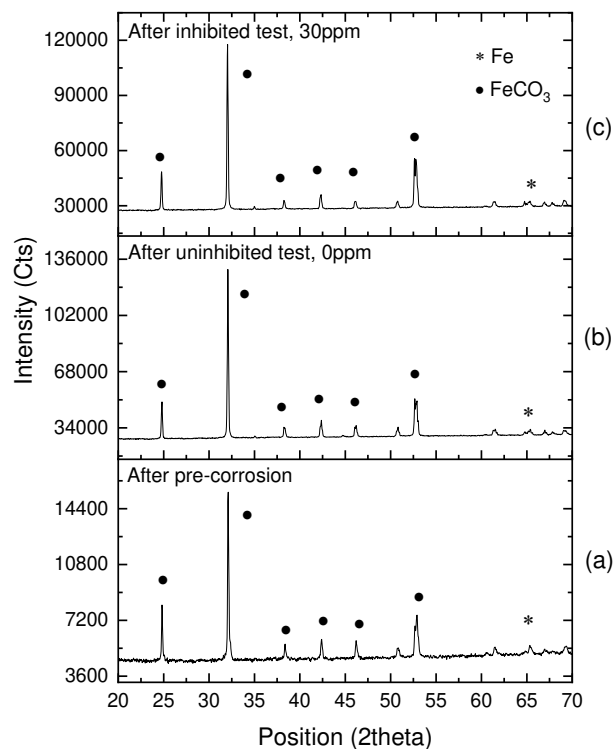


**Figure 17: XRD patterns for (a) X65 carbon steel specimen fully covered with  $\text{FeCO}_3$  after 96 h pre-corrosion in autoclave at 80°C, (b) 96 h pre-corroded specimen after exposure to uninhibited 3 wt.% NaCl brine at 80°C for 48 h and (c) 96 h pre-corroded specimen after exposure to inhibited (30 ppm) 3 wt.% NaCl brine at 80°C for 48 h**

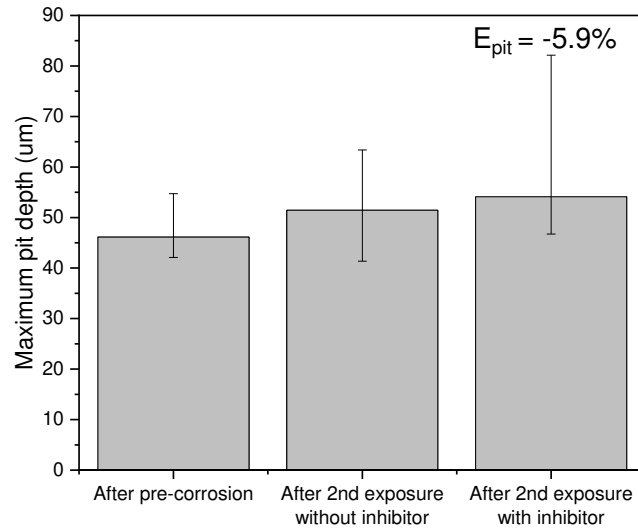


**Figure 18: Pit depth for full coverage  $\text{FeCO}_3$  layer after 96 h pre-corrosion in autoclave at 80°C, full coverage  $\text{FeCO}_3$  layer after uninhibited exposure to 3 wt.% NaCl brine at 80°C for 48 h and full coverage  $\text{FeCO}_3$  layer after exposure to inhibited (30 ppm) 3 wt.% NaCl brine at 80°C for 48 h**

### 3.5 Overall performance comparison

In section 3.1-3.4 the inhibitor efficiency of the uniform corrosion behaviour has been referred to as an end-point efficiency which is the efficiency of the corrosion inhibitor based on the final corrosion rate, assuming that there is an immediate drop in uniform corrosion rates in the presence of the inhibitor. This method is very useful as long as the time required for adsorption and film formation is considered. However, there is another approach which may be used for determining the overall efficiency of the inhibitor in terms of the uniform corrosion behaviour, i.e. integrated efficiency. The integrated efficiency provides an overall time-averaged efficiency of the corrosion inhibitor which may be more useful when describing and comparing efficiencies as it takes into account the adsorption kinetics. The end-point efficiencies and integrated efficiencies (Figure 19(a)) of the inhibited glass cell tests for wet-ground and pre-corroded X65 steel were determined using Eq. 1 and 2 respectively. The comparison of the two methods for determining the inhibitor efficiency (Figure 19) shows that the integrated efficiencies were very similar to the end-point efficiencies, apart from the 96 h pre-corroded X65 specimens, where the integrated efficiency was 57% as compared to an end-point efficiency of 83%. This was due to a massive reduction in the rate of adsorption of the corrosion inhibitor which was caused by the greater coverage and more protective nature of the  $\text{FeCO}_3$  corrosion product layer.

However as the inhibitor has been tested on pre-corroded X65 carbon steel which had corrosion product layers, the inhibitor efficiencies previously discussed (Figure 19(a)) reflect the overall protection afforded by both the inhibitor and the corrosion product. In an attempt to determine the individual protection afforded by the inhibitor and the corrosion products, the efficiency of the corrosion products in relation to protection provided was calculated relative to the corrosion rate of the uninhibited glass cell test of wet-ground X65 steel. These were then subtracted from the total efficiency to estimate the amount of protection afforded by the corrosion inhibitor on pre-corroded X65 specimens (Figure 19(b)). The total efficiency was calculated using Eq. 1 and Eq. 4 and 5 were used to calculate the individual protection afforded by the corrosion product and inhibitor, respectively.

$$E_{CP}(\%) = \left[ 1 - \left( \frac{R_{P,Uninhibited CP}}{R_{P,Uninhibited X65}} \right) \right] \times 100 \quad Eq. 4$$

$$E_{Inhibitor}(\%) = E_{Endpoint} - E_{CP} \quad Eq. 5$$

where  $E_{CP}$  is the protection afforded by the corrosion product,  $R_{P,Uninhibited CP}$  is the uninhibited polarisation resistance in the presence of the corrosion product at the end of the test,  $R_{P,Uninhibited X65}$  is the uninhibited polarisation resistance of wet-ground X65 at the end of the test,  $E_{Inhibitor}$  is the protection afforded by the corrosion inhibitor and  $E_{Endpoint}$  is the total protection afforded by the inhibitor and corrosion product (Eq. 1).

However, as previously discussed, all corrosion products had undergone some extent of dissolution which meant that the data provided (Figure 19(b)) had underestimated the inhibitor contribution towards overall corrosion protection and overestimated the overall corrosion protection afforded by the corrosion products. In spite of this, the data (Figure 19(b)) provide an indication as to how the individual contributions of the corrosion product and the inhibitor change with increasing pre-corrosion time (i.e. more protective corrosion product layers). The data show that the presence of  $Fe_3C$  had resulted in slightly improved adsorption kinetics and improved overall protection against uniform corrosion by the end of the inhibited test (as compared to wet-ground X65 steel) as shown by Figure 19 (a) and (b) which can be attributed to the greater evolution of the bulk solution pH especially during the initial stages of the inhibited test where the corrosion rates are greater in the presence of  $Fe_3C$  as compared to wet-ground X65 steel (Figure 7 and Table 3).

The adsorption kinetics of the corrosion inhibitor was further diminished in the presence of the partially covered  $FeCO_3$  surface (Figure 11) which is due to the inhibitor being unable to adsorb onto water-wetted  $FeCO_3$  [19]. Contact angle measurements showed that when the wet-ground

steel is initially in contact with oil or water, additions of >10 and up to 100 ppm corrosion inhibitor create an oleophilic surface indicating strong inhibitor adsorption and film formation. In sharp contrast, particularly when in contact with water, the  $\text{FeCO}_3$  surface is hydrophilic and remains hydrophilic on the addition of >10 and up to 100 ppm inhibitor [19]. However by the end of the corrosion test, the protection afforded against uniform corrosion had increased by 4% (compared to wet-ground X65) as shown by Figure 19(a). This can be attributed to the increase in bulk solution pH caused by the dissolution of  $\text{FeCO}_3$  during the inhibited test (Figure 11). Figure 19(b) indicates that 43% of the overall protection was afforded by the partial coverage of  $\text{FeCO}_3$  and the remainder by the corrosion inhibitor. The integrated efficiency had also reduced by 1.3% as compared to 6 h pre-corrosion and was 1.6% lower than the end-point efficiency indicating slower adsorption kinetics as previously indicated by Figure 11(a). This slower rate of adsorption coupled with the nature of the protective film indicated that although the end-point efficiency was similar to that of 6 h pre-corroded X65 steel, this coupled effect gave rise to more severe localised corrosion attack which is more difficult to control at the same relative inhibitor dosage. However as the partial coverage of  $\text{FeCO}_3$  had completely dissolved by the end of the inhibited test, it can be concluded that the majority of protection afforded with respect to uniform corrosion by the end of the 48 h inhibited test was due to the corrosion inhibitor.

Similarly, for the fully covered  $\text{FeCO}_3$  surface, the adsorption kinetics were slower however with a lower end-point efficiency of 83% and a much lower integrated efficiency of 57% (Figure 19(a)). In this case the majority of the protection against uniform corrosion was afforded by the full coverage of  $\text{FeCO}_3$  rather than by the corrosion inhibitor which was due to its protective nature and the extremely slow dissolution rate of the  $\text{FeCO}_3$  layer (Figure 16). However, as previously observed and discussed for 24 h pre-corroded X65 steel, the nature of the 96 h pre-corroded X65 steel has a dramatic influence on the adsorption kinetics of the corrosion inhibitor which when coupled together give rise to more severe localised corrosion attack.

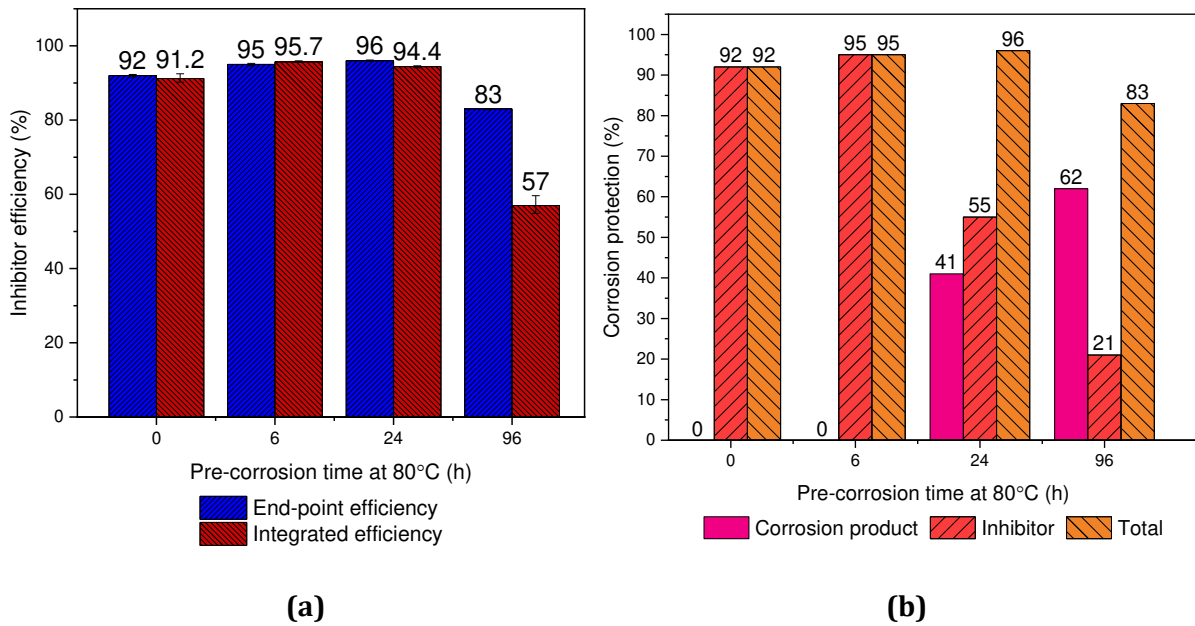


**Figure 19: (a) Uniform corrosion inhibitor efficiencies and (b) estimation of individual corrosion protection afforded by corrosion products and corrosion inhibitors where the pre-corrosion time of 0, 6, 24 and 96 h refer to wet-ground X65 steel, X65 steel with a Fe<sub>3</sub>C-rich layer, X65 steel with a partial coverage of FeCO<sub>3</sub> and X65 steel with a fully covered FeCO<sub>3</sub>-rich layer, respectively.**

The uniform and localised corrosion efficiencies were compared (Figure 20) for all the pre-corrosion times in order to evaluate the optimum pre-corrosion time for maximum protection against both uniform and localised corrosion. The data indicated that although 24 h of pre-corrosion (partially covered FeCO<sub>3</sub>) resulted in the highest inhibitor efficiency with respect to the uniform corrosion behaviour (96%), the highest set of uniform and localised corrosion efficiencies was for zero hours of pre-corrosion which meant that the imidazoline corrosion inhibitor provided optimum corrosion protection on wet-ground X65 carbon steel. Figure 20 also indicates that severe localised corrosion attack is prevalent in the presence of FeCO<sub>3</sub>, whether or not it covers the entire steel surface. This dramatic reduction in the inhibitor's ability to retard localised corrosion attack in the presence of both partial/full coverage FeCO<sub>3</sub> is due to the inhibitor's inability to adsorb under or on FeCO<sub>3</sub> crystals which was not aided by the slow dissolution of FeCO<sub>3</sub> resulting in an increase in both single crystal porosity and porosity between crystal grains (Figure 16).

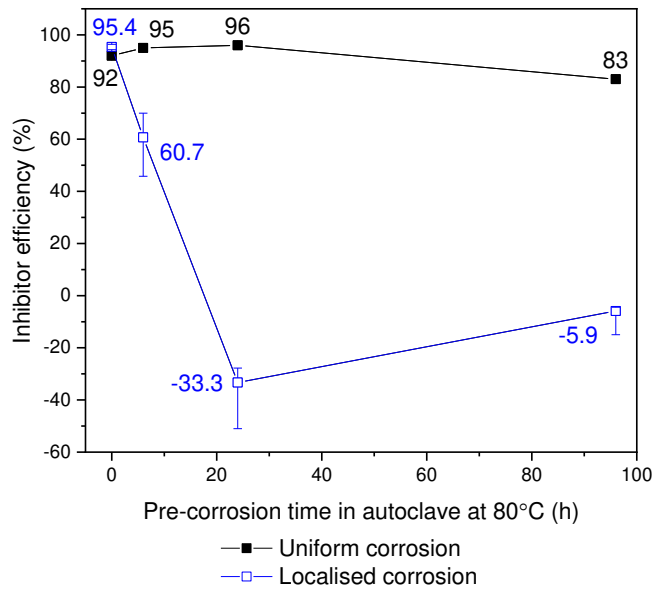


**Figure 20: Uniform and localised corrosion inhibitor efficiency comparison for wet-ground X65, Fe<sub>3</sub>C-rich layer (6 h pre-corrosion), partial coverage FeCO<sub>3</sub> (24 h pre-corrosion) and full coverage FeCO<sub>3</sub> (96 h pre-corrosion)**

#### 4.0 Conclusions

The performance of an imidazoline corrosion inhibitor on pre-corroded X65 carbon steel was assessed and compared to its performance on wet-ground X65 carbon steel with respect to both uniform and localised corrosion behaviour. Pre-corrosion in autoclaves at 80°C for 6, 24 and 96 h led to the exposure of Fe<sub>3</sub>C, and precipitation of a FeCO<sub>3</sub>-rich layer which provided partial coverage and a FeCO<sub>3</sub>-rich layer with high coverage of the steel surface, which were transferred and tested in glass cell tests using both uninhibited and inhibited CO<sub>2</sub>-saturated brines.

The imidazoline corrosion inhibitor was found to increase the rate of dissolution of FeCO<sub>3</sub> which is one of its roles when used in oil and gas production fluid environments, as it helps prevent corrosion product growth. Corrosion protection was found to be a function of two factors, inhibitor adsorption/film formation and the presence of corrosion products. This effect was most significant in the presence of a FeCO<sub>3</sub>-rich layer with high coverage of the steel surface, resulting in the inhibitor providing only 25% of the overall protection afforded by the corrosion inhibitor and corrosion product. Taking into consideration corrosion suppression of both uniform and localised attack, the imidazoline inhibitor was most efficient in the absence of any corrosion products (fresh ground surface) and least efficient in the presence of crystalline FeCO<sub>3</sub>, where the nature of the steel surface in the presence of FeCO<sub>3</sub> had a significant influence on the adsorption

kinetics of the corrosion inhibitor which when coupled together gave rise to more severe localised corrosion attack.

## 5.0 Data availability

The raw/processed data required to reproduce these findings cannot be shared at this time as the data also forms part of an ongoing study.

## 6.0 References

1. Rahuma, M. and M. Bobby Kannan, *Corrosion in Oil and Gas Industry: A Perspective on Corrosion Inhibitors*. J Material Sci Eng, 2014. p. 110.
2. Shamsa, A., R. Barker, Y. Hua, E. Barmatov, T.L. Hughes, and A. Neville, *The role of  $Ca^{2+}$  ions on Ca/Fe carbonate products on X65 carbon steel in  $CO_2$  corrosion environments at 80 and 150° C*. 2019. p. 58-70.
3. Rahuma, M.N., M.B. EL-Sabbah, and I.M. Hamad, *Effect of Serine and Methionine on Electrochemical Behavior of the Corrosion of Mild Steel in Aqueous Solutions*. ISRN Corrosion, 2013.
4. Miksic, B.M., A.Y. Furman, and M.A. Kharshan, *Effectiveness of the corrosion inhibitors for the petroleum industry under various flow conditions*. CORROSION 2009, 2009.
5. Arnold, R., D.B. Burnett, J. Elphick, T. Feeley, M. Galbrun, M. Hightower, Z. Jiang, M. Khan, M. Lavery, and F. Luffey, *Managing water—from waste to resource*. Oilfield Review, 2004. p. 26-41.
6. Barker, R., I. Al Shaaili, R. De Motte, D. Burkle, T. Charpentier, S. Vargas, and A. Neville, *Iron carbonate formation kinetics onto corroding and pre-filmed carbon steel surfaces in carbon dioxide corrosion environments*. Applied Surface Science, 2019. p. 135-145.
7. Barker, R., D. Burkle, T. Charpentier, H. Thompson, and A. Neville, *A review of iron carbonate ( $FeCO_3$ ) formation in the oil and gas industry*. Corrosion Science, 2018. p. 312-341.
8. Barker, R., Y. Hua, and A. Neville, *Internal corrosion of carbon steel pipelines for dense-phase  $CO_2$  transport in carbon capture and storage (CCS)—a review*. International Materials Reviews, 2017. p. 1-31.
9. Fink, J., *Clay Stabilization. Chapter 3*. Petroleum Engineer's Guide to Oil Field Chemicals and Fluids. Gulf Publishing Company, Houston, Texas, USA, 2012. p. 125-137.
10. Palencsár, A., E. Gulbrandsen, and K. Kosorú. *High Temperature Testing of Corrosion Inhibitor Performance*. in *CORROSION 2013*. 2013. NACE International.
11. Jenkins, A. *Performance of High-Temperature, Biodegradable Corrosion Inhibitors*. in *CORROSION 2011*. 2011. NACE International.
12. Gulbrandsen, E., S. Nestic, S. Morten Hesjevik, S. Skjerve, B. Sundfer, T. Burchardt, and A. Stangeland, *Effect of precorrosion on the performance of inhibitors for  $CO_2$  corrosion of carbon steel*. CORROSION 98, 1998.
13. Paolinelli, L., T. Pérez, and S. Simison, *The effect of pre-corrosion and steel microstructure on inhibitor performance in  $CO_2$  corrosion*. Corrosion Science, 2008. p. 2456-2464.
14. Zhang, H.-h., X. Pang, M. Zhou, C. Liu, L. Wei, and K. Gao, *The behavior of pre-corrosion effect on the performance of imidazoline-based inhibitor in 3 wt.% NaCl solution saturated with  $CO_2$* . Applied Surface Science, 2015. p. 63-72.
15. Al-Asadi, A.A., *Iron Carbide Development and its Effect on Inhibitor Performance*. 2014, Ohio University.
16. Chokshi, K., *A Study of Inhibitor-Scale Interaction in Carbon dioxide Corrosion of Mild Steel*. 2004, Ohio University.

17. ASTM, G., *G 1-03. Standard Practice for Preparing, Cleaning, and Evaluating Corrosion Test Specimens,* Philadelphia, Pennsylvania: American Society for Testing and Materials, 2003.
18. Shamsa, A., R. Barker, Y. Hua, E. Barmatov, T.L. Hughes, and A. Neville, *Performance evaluation of an imidazoline corrosion inhibitor in a CO<sub>2</sub>-saturated environment with emphasis on localised corrosion.* Corrosion Science, 2020: p. 108916.
19. Shamsa, A., *Corrosion Product Growth Kinetics/Characteristics and Inhibitor Performance in CO<sub>2</sub> Environments.* 2019, University of Leeds.